Relationship of F-actin Distribution to Development of Polar Shape in Human Polymorphonuclear Neutrophils

Thomas D. Coates,* Raymond G. Watts,‡ Raymond Hartman,* and Thomas H. Howard‡§

*The Division of Pediatric Hematology/Oncology at Childrens Hospital Los Angeles, University of Southern California, Los Angeles, California; and ‡the Division of Pediatric Hematology/Oncology and §the Department of Cell Biology, The University of Alabama, Birmingham, Alabama

Abstract. Polymerization of actin has been associated with development of polar shape in human neutrophils (PMN). To examine the relation of filamentous actin (F-actin) distribution to shape change in PMN, we developed a method using computerized video image analysis and fluorescence microscopy to quantify distribution of F-actin in single cells. PMN were labeled with fluorescent probe NBD-phallicidin to measure filamentous actin and Texas red to assess cell thickness. We show that Texas red fluorescence is a reasonable measure of cell thickness and that correction of the NBD-phallicidin image for cell thickness using the Texas red image permits assessment of focal F-actin content. Parameters were derived that quantify total F-actin content, movement of F-actin away from the center of the cell, asymmetry of F-actin distribution, and change from round to polar shape. The sequence of change in F-actin distribution and its relation to development of polar shape in PMN was determined using these parameters. After stimulation with chemotactic peptide at 25°C, F-actin polymerized first at the rim of the PMN. This was followed by development of asymmetry of F-actin distribution and change to polar shape. The dominant pseudopod developed first in the region of lower F-actin concentration followed later by polymerization of actin in the end of the developed pseudopod. Asymmetric F-actin distribution was detected in round PMN before development of polar shape. Based upon these data, asymmetric distribution of F-actin is coincident with and probably precedes development of polar shape in PMN stimulated in suspension by chemotactic peptide.

SHAPE is a distinctive and sufficiently unique feature of cells to allow their identification and morphologic classification. Since form follows function, the shape adopted by single cells or cells within a tissue is usually adapted to the specific functions of those cells. For example, morphologic polarity of epithelial cells underlies functional and biochemical polarities which coordinate bidirectional transport (33). In tissue, the morphologic polarity of cells is maintained by cell-to-cell contacts and by intrinsic organization of microfilamentous cytoskeleton. The study of shape acquisition and shape change by cells is therefore of critical importance to understanding cell function.

Functionally important morphologic polarization also occurs when single cells like polymorphonuclear neutrophils (PMN)[1] are stimulated. On surfaces and in a gradient of chemotactic factor, PMN acquire a polar shape and develop pseudopods which align with the gradient (37). However, the same polarization response occurs in the absence of either a gradient or attachment to a surface (35). In suspension, basal PMN are spherical and smooth with no membrane ruffling but, when stimulated by chemotactic agents, they elongate and develop a polar shape similar to that of attached cells. Therefore, the biochemical and force-generating events necessary for the polarization response induced by chemotactic factors must be intrinsic to the cells.

In the studies presented here, we used the chemotactic factor–activated PMN, in suspension, as a model to examine the role of the microfilamentous cytoskeleton in determining cell shape. Actin, the main component of the microfilamentous cytoskeleton, exists as monomeric globular actin which polymerizes to form filamentous actin (F-actin). Other proteins such as actin-binding proteins interact with globular actin and F-actin to regulate the structure of the microfilamentous cytoskeleton (28). The microfilamentous cytoskeleton of PMN activated by chemotactic factors or by substrate contact is constantly remodeled through actin polymerization and F-actin depolymerization (5, 27). Changes in F-actin content at any time or in any region within the cell reflect the balance between these two processes. These changes have been associated with dynamic reorganization of microfilamentous cytoskeleton and polarization in some cells (8, 32). After activation, PMN change shape from round to polar, serially increase and decrease F-actin content, and apparently shift F-actin distribution from diffuse to focal (15).

1. *Abbreviations used in this paper*: FMLP, n-formyl-methionyl-leucyl-phenylanine; NBD-phal, NBD-phallacidin; PMN, polymorphonuclear neutrophils; TR, Texas red.

These observations suggest that the amount and distribution of F-actin may play an important role in the development or maintenance of PMN shape. However, the evidence which supports this idea is circumstantial and derives primarily from fluorescence microscopy studies which localize F-actin to the subcortical region of the pseudopod of PMN or other cells (11, 15, 22). These studies do not establish a cause- and -effect relationship between presence of F-actin and development of a pseudopod. To date, no study of cytoskeleton and shape uses a round cell which can assume any shape to directly examine the relationship between temporal change in microfilamentous cytoskeleton organization and acquisition of shape.

To determine whether F-actin distribution is critical for development of polar shape, we described the temporal relationship between F-actin distribution and change in shape of activated PMN. This requires adequate methodology to define the cell boundary and to determine focal F-actin concentrations in a manner independent of cell thickness. Therefore, we used Texas red (TR) staining of protein to develop a ratio imaging technique which corrects fluorescent microscopic images of NBD-phallacidin–labeled (NBD-phal) PMN for variation in cell thickness. The resulting ratio images are two-dimensional projections of cells which reflect focal F-actin concentration. We also developed simple mathematical parameters which quantitatively describe F-actin content, F-actin distribution, and shape of single PMN. After stimulation, these parameters were measured in PMN at 5-s intervals with an image analysis system which permits automatic analysis of large numbers of cells.

Kinetic analysis of F-actin and PMN shape after stimulation with the chemotactic peptide, *n*-formyl-methionyl-leucyl-phenylalanine (FMLP) shows that focal changes in the state of actin polymerization are intimately related to changes in PMN shape. Specifically, the initial increase in F-actin is associated with symmetric accumulation of F-actin at the cell periphery. This is followed by the development of asymmetric F-actin distribution away from the geographic center of the cell and, lastly, by change from a spherical to a polar shape. The kinetic data show that asymmetric distribution of F-actin occurs even in round cells and suggest that the asymmetric distribution which precedes the acquisition of polar shape may be causally related to shape change and pseudopod formation in PMN. Based upon these data, we are able to formulate a model for the participation of focal polymerization/depolymerization of actin in the development of polar shape in human PMN.

Materials and Methods

Reagents

The following reagents were used for the studies outlined below: TR, NBD-phal, and FURA-2 (Molecular Probes Inc., Junction City, OR); FMLP and lysophosphatidylcholine (Sigma Chem. Co., St. Louis, MO); and Percoll (Pharmacia LKB Biotechnology Inc., Piscataway, NJ).

Cell Preparation

Human PMN were purified from the peripheral blood of normal volunteer donors as approved by the Committee on Human Investigation at Childrens Hospital Los Angeles and the Internal Review Board of the University of Alabama at Birmingham. The blood was collected and the cells were prepared on endotoxin-free Percoll gradients in autologous plasma as previously described (18, 35). The method yields a 98% pure PMN suspension, endotoxin free (lipopolysaccharide <12 pg/ml solution). The purified cells were suspended in Hanks'/Hepes balanced buffer with calcium and magnesium (25 mM Hepes, 50 mM phosphate, 150 mM NaCl, 4 mM KCl, 1.0 mM $MgCl_2$, 1.2 mM $CaCl_2$ pH 7.15) and were studied in suspension within 1 h of purification (15, 16, 35).

Stimulation, Fixation, and Staining

Neutrophils (250 μl) at 4×10^6 cells/ml in buffer were stimulated at 25°C by addition of equal volume of buffer containing 0.0001 vol% DMSO or 2×10^{-9} M FMLP for the indicated periods of time and then fixed with 50 μl of 37% formalin for 10 min. PMN were permeabilized with lysophosphatidylcholine (80 μg/ml) and stained with NBD-phal (3.3×10^{-7}M) for 15 min. TR (7 μl of 1 mg TR/ml in dimethylformamide) was added to the PMN in NBD-phal fixation buffer; the cells were immediately sedimented (400 *g* for 5 min) and washed twice in 15 cc of buffer or 0.9% NaCl. Aliquots of PMN were then laid onto coverslips (1,000 rpm for 5 min) in a Cytospin II (Shandon Inc., Pittsburgh, PA), air dried, and held in the dark until preparation for fluorescence microscopy. To test if air drying altered the distribution of F-actin, PMN were stimulated with 10^{-9} M FMLP and sampled at 0, 20, 45, 90, and 300 s. The cells were labeled and spun onto slides. Half of the slides were allowed to air dry and half were mounted in glycerol without being allowed to dry. When examined visually and when 363 PMN were quantitated as described here, there were no differences in the fluorescence distribution between the wet and dry preparations ($p < 0.28$). In experiments confirming registration of red and green images, the cells were overlaid with a 1:10,000 dilution of 0.2-μm-diam, polychromatic (TR and fluorescein) Fluorobrite beads (Polysciences Inc., Warrington, PA) such that beads were evenly distributed at a density of 0–2 beads/40× microscopic field. The cells were then mounted in 90% glycerol in PBS for microscopy.

Generation of Raw Texas and NBD-phal Images

Unless otherwise specified, PMN were imaged using a Nikon MicroPhot microscope with a 40× Neofluor oil immersion phase objective and a 1.25× intermediate lens. The NBD-phal and TR images were obtained using an Omega Optical filter block with custom-designed dichroic mirror having passbands of 450–480 nm and 505–555 nm. The excitation filter has pass bands at 530 and 570 nm. A 530 ± 20 nm interference filter was used in the emission path for NBD-phal images and a 590-nm long-pass filter was used for TR. There was no NBD-phal fluorescence detected with the TR filter setup nor TR fluorescence detected with the NBD-phal filter setup.

Images were taken with an instrumentation camera (model 70; Dage-MTI, Inc., Michigan City, IN) and a Videoscope (Video Scope Intl. Ltd., Washington, DC) image intensifier. The camera output and the computer video output were continuously monitored on an oscilloscope to assure that the signals remained in the linear operating range of the amplifiers. Each field was averaged 32 times and stored for later analysis on an optical disk recorder (TQ-2027F; Panasonic Industrial Co., Secaucus, NJ). The image analysis system consists of three planes of $512 \times 512 \times 256$ image memory, analog-to-digital converter, arithmetic logic unit (Imaging Technology, NJ), IRIS 2400 minicomputer (Silicon Graphics, Mountainview, CA), and a basic image analysis software library (GW Hannaway and Associates, Boulder, CO). Additional specific routines for the functions described here were written by the authors.

Optical sectioning microscopy was performed using software (Micro-Tome II; Vay-Tek, Inc., Fairfield, IA) which determines the point-spread function of the microscope and then uses this function to remove out-of-focus information above and below the plane of focus.

There is very little photobleaching of the TR image over a period of 10 s; however, the NBD-phal image undergoes a ~10% decrease during the same period. To minimize variability due to photobleaching, only four fields per slide were selected and the duration of exposure of the stained cells to the excitation light was controlled by the computer.

The edge of the TR image was used to define the edge of the cell. The ability of TR to detect the thinnest region of the cell edges was determined at 100× on spread PMN by comparison of the TR image with the edge determined by differential interference contrast or phase microscopy (see Results). No detectable error in magnification due to a difference in wavelength between the red and green images was observed (4).

Generation of Processed TR, NBD-phal, and NBD-phal/TR Ratioed Images

Backgrounds were subtracted from the TR and NBD-phal images before the ratio image was calculated. The x,y coordinates of the points comprising

the edge of the TR image of each cell were automatically determined by a feature extracting program and stored in a file for each cell. Another program, which implements the calculations below, subsequently uses these files which define the cell boundary. The alignment of the TR and NBD-phal images was tested by placing a Fluoresbrite bead in the field with the PMN. The bead is uniformly fluorescent and can be seen both with the TR and NBD-phal filter configurations. A consistent error of ~2 pixels in the x and y direction was found in the alignment of the TR and NBD-phal images. The images were aligned based upon the placement of the bead and the NBD-phal image was then divided by the TR image. Once the images were stored to optical disk and the identifying data stored in an experiment log file, a specific routine automatically finds the PMN, forms the ratio image, and produces a data file containing the distribution parameters and the associated experimental condition (time, concentration, etc.). Thus, no operator bias was introduced in the selection of the images to study.

Mathematical Definition of Parameters

A morphometry program was written to calculate various parameters from the ratio image. The cell edge used for these calculations was determined from the corresponding TR image. For each of the equations, the summations are carried out for all points (picture elements or "pixels") $x_n y_n$ within the cell boundary. i_{xy} is the intensity of the n^{th} pixel at position $x_n y_n$. N is the number of pixels within the cell boundary and is thus equal to the area of the cell image. The scalar I_t is the sum of the intensity of all pixels within the cell boundary. The geometric center (Eq. 1) of the cell is located at $x_g y_g$ and is determined by calculating the average x and y coordinates from the set of all points within the cell edge of the TR image (Fig. 1).

$$x_g = \frac{\sum_1^N x_n}{N} \quad y_g = \frac{\sum_1^N y_n}{N} \tag{1}$$

The intensity center (Eq. 2) of the cell is located at x_i, y_i and is calculated in a similar fashion except that the x,y coordinates are weighted by the intensity (i_{xy}) at each particular point.

$$x_i = \frac{\sum_1^N i_{xy} x_n}{\sum_1^N i_{xy}} \quad y_i = \frac{\sum_1^N i_{xy} y_n}{\sum_1^N i_{xy}} \tag{2}$$

$$ASYM = \Sigma \sqrt{(x_i - x_g)^2 + (y_i - y_g)^2} \tag{3}$$

Asymmetry (*ASYM*; Eq. 3) is the distance from x_g, y_g to x_i, y_i and measures the net shift of the center of fluorescence from the geometric center of the cell. Since some cells exhibited symmetrically distributed focal regions of fluorescence, we derived a related parameter that measures symmetric movement of fluorescence away from the center of the cell. This parameter, radial dispersion (*RD*; Eq. 4) is distinct from *ASYM* and represents the distance from the geometric center of the cell, $x_g y_g$, to a narrow ring of fluorescence, Δr, whose intensity is equal to the total intensity (I_t). *RD* is a measure of distribution of fluorescence away from the cell center whether symmetric or asymmetric and, as shown in the results, is insensitive to total fluorescence intensity.

$$RD = \frac{\sum_1^N i_{xy} \sqrt{(x_n - x_g)^2 + (y_n - y_g)^2}}{I_t} \tag{4}$$

Ellipticity (*ELIP*; Eq. 5) is a measure of the variation from a circle of the shape of the cell. Eq. 5 is derived by dividing the measured cell area (N) by the area of a circle whose circumference is equal to the measured perimeter (p) of the cell (15).

$$ELIP = \frac{4\pi N}{p^2} \tag{5}$$

The intensity vector $\bar{I}$ at the geometric center points toward the intensity center, and has a length equal to *ASYM* (Fig. 1). $\bar{I}_{TR}$ and $\bar{I}_{ratio}$ are the vectors for the respective TR image and NBD-phal/TR images. The vector dot product, P, of the two vectors $\bar{I}_{TR}$ and $\bar{I}_{ratio}$ is defined as $|\bar{I}_{TR}| \times |\bar{I}_{ratio}| \cos\theta$, where θ is the angle between the two vectors. The dot product was calculated from the geometric center and the intensity center of the respective images by simple vector algebra (1) (Eq. 6).

$$P = (X_g^{TR} - X_i^{TR})(X_g^{ratio} - X_i^{ratio}) + (Y_g^{TR} - Y_i^{TR})(Y_g^{ratio} - Y_i^{ratio}) \tag{6}$$

The dot product is >0 if the vectors point in the same direction and <0 if they point opposite.

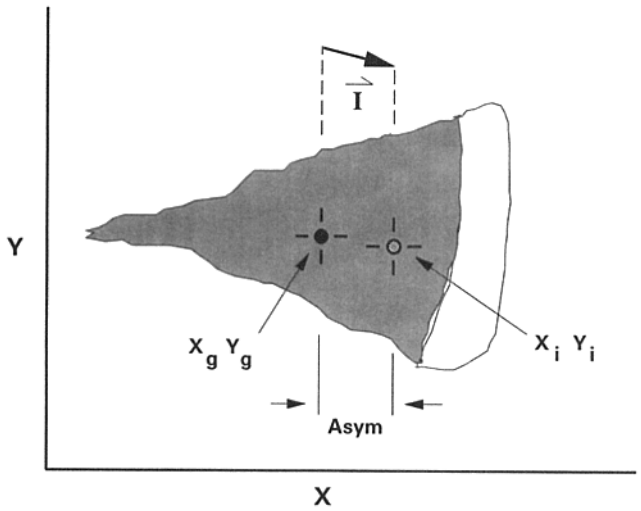

Figure 1. Schematic diagram of a polarized neutrophil with F-actin concentrated at the right. The geometric center, X_g,Y_g, and intensity center, X_i,Y_i, are indicated. The intensity vector, $\bar{I}$, points from the geometric center to the intensity center and has a length equal to *ASYM*.

Data Analysis

Differences between means were tested by analysis of variance or t test. Differences in medians were tested by the median test or Wilcoxon rank sum test. Because of significant day-to-day variation, representative data from a single experiment consisting of analysis of 1,500 PMN are presented here. Similar results were obtained in three other experiments. To permit presentation on the same scale, fluorescence parameters expressed were normalized to their respective maximum values.

Results

The TR Image Defines Cell Edge, Geometric Center, and Cell Thickness

TR binds to lysine amino groups of proteins (13) and has a fluorescent spectrum which permits double staining with the F-actin probe, NBD-phal. PMN have no fixed anatomic point that can easily be used as a reference for imaging studies. Therefore, we chose the geometric center of the cell, calculated from the cell boundary, as a reference point on the cell. Because the computer can automatically and more easily find the edge of a fluorescent image than that of a phase image, the cell edge was defined as the edge of the TR image for studies presented here. When compared to the phase image, the intensity of TR fluorescence at the edge is sufficient, even at the thinnest regions, to accurately define the edge of the PMN which had spread on a glass surface. A similar correspondence between phase or differential interference contrast image and TR image was seen with cells stained in suspension and then spun onto slides with a cytocentrifuge. Thus, the edge detected by TR fluorescence is a good representation of the PMN edge.

Since the microscopic image of a fluorescently labeled PMN is a two-dimensional projection of a three-dimensional object, localized variations in fluorescence intensity may be due to regional differences in thickness within the cell (i.e., variations in "pathlength") (4). The TR image was used to compensate for variations in cell thickness. To use the TR fluorescence as a measure of thickness, the concentration of the probe must be low enough to be nonquenching and

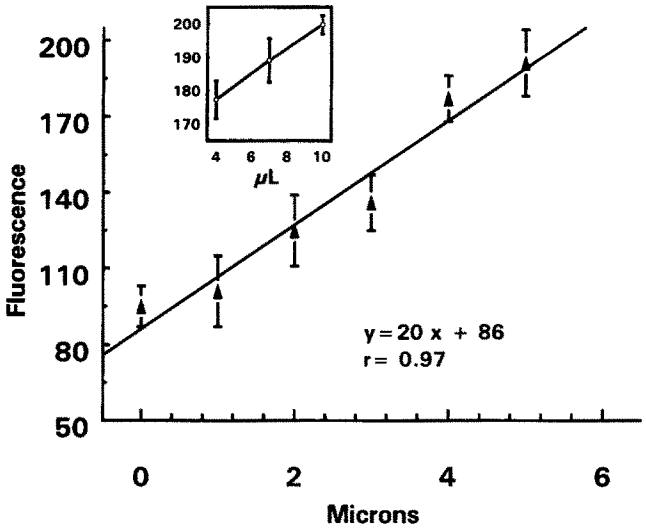

Figure 2. Linearity of TR fluorescence and use of TR fluorescence as a measure of cell thickness. To quantify TR fluorescence, images were taken at 1-μm planes of focus and the out-of-focus fluorescence was removed. TR fluorescence was then measured on the whole cell image at the points on the edge of each section and the TR fluorescence (▲) was plotted against the known depth of the respective section. In the inset, ○ demonstrates the linear relation of total TR fluorescence in PMN to the volume (μl) of TR stock solution used to stain the PMN.

linearly related to cell thickness. Fig. 2 (*inset*) demonstrates that TR staining is linear over the range of concentrations of dye used in these experiments. This relation is linear in cells double stained with NBD-phal and TR. Optical sectioning microscopy was used to confirm the relation of TR intensity to thickness (14). TR-labeled PMN were imaged at 1-μm planes of focus and the out-of-focus fluorescence was removed electronically. This resulted in six images or "slices" through the PMN parallel to the microscope slide and spaced 1 μm apart. The edge of the PMN in each section was determined. When these edge files were overlaid on the original images, they identify the points on the image that are equidistant from the microscope slide at a distance corresponding to the position of slice from which the particular edge file was obtained. Measurements of the intensity at the points on these edges overlaid on the whole cell TR image were plotted against the position of the respective edge. Fig. 2 shows the linear relation of TR intensity to cell thickness which results from this procedure. Under the conditions of these experiments, TR fluorescence was bright enough to visualize thin regions, was not self-quenching, was a reasonably linear measure of cell thickness and, therefore, is suitable for measurements of edge and thickness. It should be noted that TR estimates the "protein space," including organelles.

Ratio Images of NBD-phal/TR Reflect Focal F-actin Concentration

NBD-phal and TR images of PMN were separately obtained, perfectly aligned, and corrected for background fluorescence. The NBD-phal image (F-actin) was then divided point for point by the TR image (cell thickness). Thus, the intensity at each point of the ratio image represents the amount of F-actin per unit protein at that point. Fig. 3 demonstrates the effect of correcting the NBD-phal image for thickness. There is a clear difference in the F-actin distribution assessed from the ratio image (*top*) and that deduced from the direct NBD-phal image which one would see with standard fluorescence microscopy (*middle*). This difference demonstrates the importance of correcting NBD-phal fluorescence for estimated cell thickness. As illustrated in Fig. 3, ratio imaging allows one to discriminate both asymmetric and symmetric F-actin distributions that are not evident by standard fluorescence microscopy. Furthermore, it permits detection of asymmetry of F-actin in even round cells (Fig. 4, cell B).

Definition and Validation of Parameters of Shape and F-actin Distribution

The parameters used to quantitatively describe shape and spatial distribution of F-actin were determined on NBD-phal/TR ratio images of PMN. The mathematical definitions for these parameters are presented in detail in Materials and Methods. The parameters are defined as follows: total cellular fluorescence (*I*) is the sum of the fluorescence intensity at each point within the cell boundary; *RD* measures any displacement of fluorescence, symmetric or asymmetric, away from the center of the cell; and *ASYM* measures only asymmetric displacement of fluorescence away from the center of the cell. *ELIP* is a measure of the variation from a circle of the shape of the cell and has previously been used in numerous studies (15, 19). *ELIP* decreases as the cell acquires polar shape.

Fig. 4 demonstrates how values for the parameters *I*, *RD*, and *ASYM* change as the fluorescence distribution changes. *I* has units of relative fluorescence intensity. *RD* and *ASYM* reflect relative changes in fluorescence distribution and have units of distance. The ratio images of PMN at various times after stimulation with FMLP were selected to demonstrate the characteristics of fluorescence distribution detected by *RD* and *ASYM*. The parameters *I*, *RD*, and *ASYM* were calculated for each of these cells. Cells D, E, and F, whose fluorescence is asymmetrically distributed, have high values of *ASYM* and *RD*. In contrast, cell A has a relatively uniform fluorescence and thus the calculated values for *ASYM* and *RD* are lower. Cells such as G and H, whose fluorescence is predominately at the cell periphery but clearly symmetric, also have low values for *ASYM* but the corresponding values of *RD* are high, thus demonstrating the sensitivity of these parameters to symmetric and asymmetric distribution of fluorescence.

Fluorescence intensity plays an important role in the calculation of the distribution parameters as well. The amount of staining and the instrument settings can affect the measurement of fluorescence intensities and therefore could influence the distribution parameters unless they are independent of *I* in the range of intensities observed in our experiments. To examine this question, *RD* and *ASYM* were measured in the original set of ratio images shown in Fig. 5 and in two additional sets of ratio images, derived from the original set but modified to have equal total intensity (Fig. 4, *hatched bars*) or a 1.5-fold increase in total intensity (Fig. 4, *solid bars*). When the results for *ASYM* and *RD* calculated from these different sets of images were compared, there was no difference between the original image (*open bars*) and the two normalized images (*hatched* and *solid bars*). This indi-

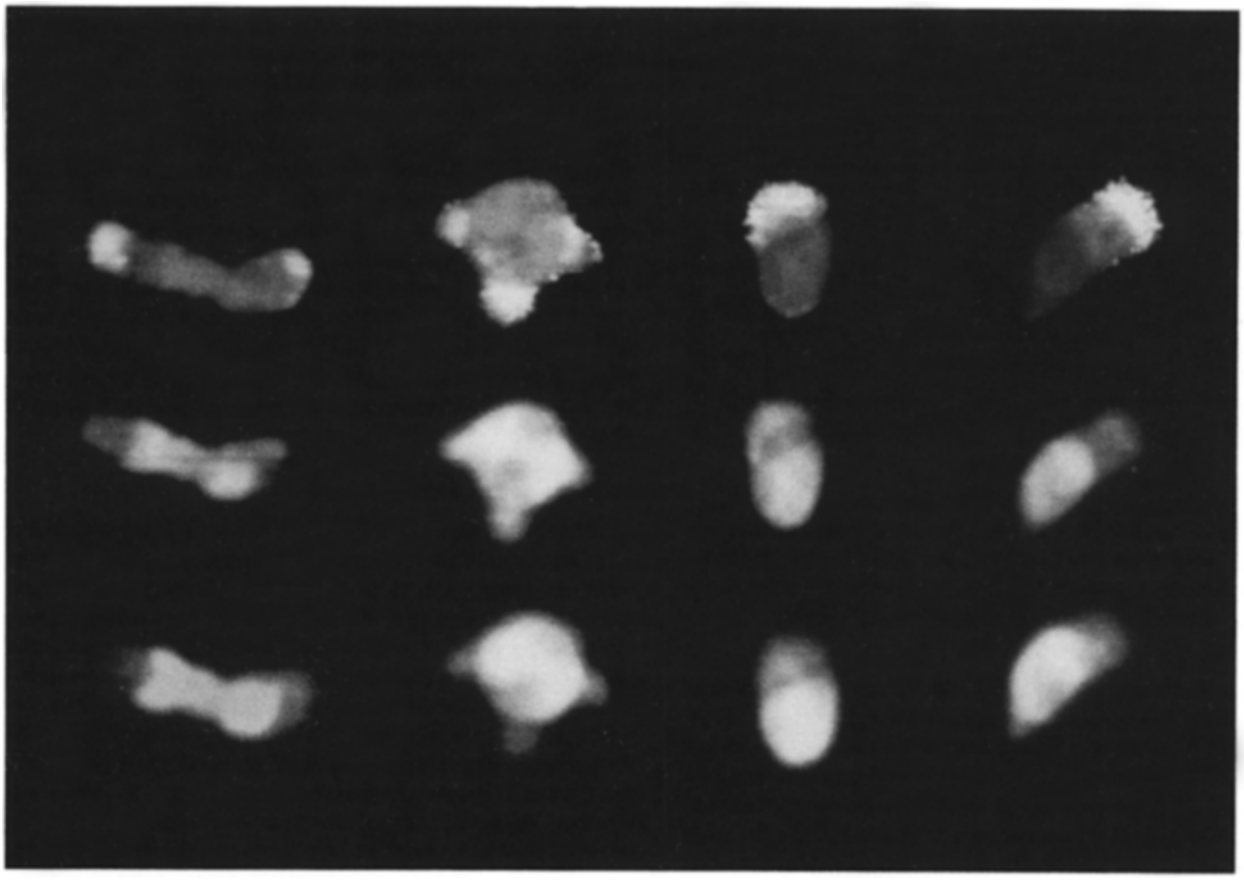

Figure 3. Illustrative ratio, NBD-phal, and TR images of PMN. The bottom row shows the TR image corresponding to the NBD-phal image in the middle row. The top row is the result of dividing the middle row by the bottom row. The figure demonstrates that the impression of F-actin distribution in the ratio image (*top*) is quite different from that seen by standard microscopy (*middle*).

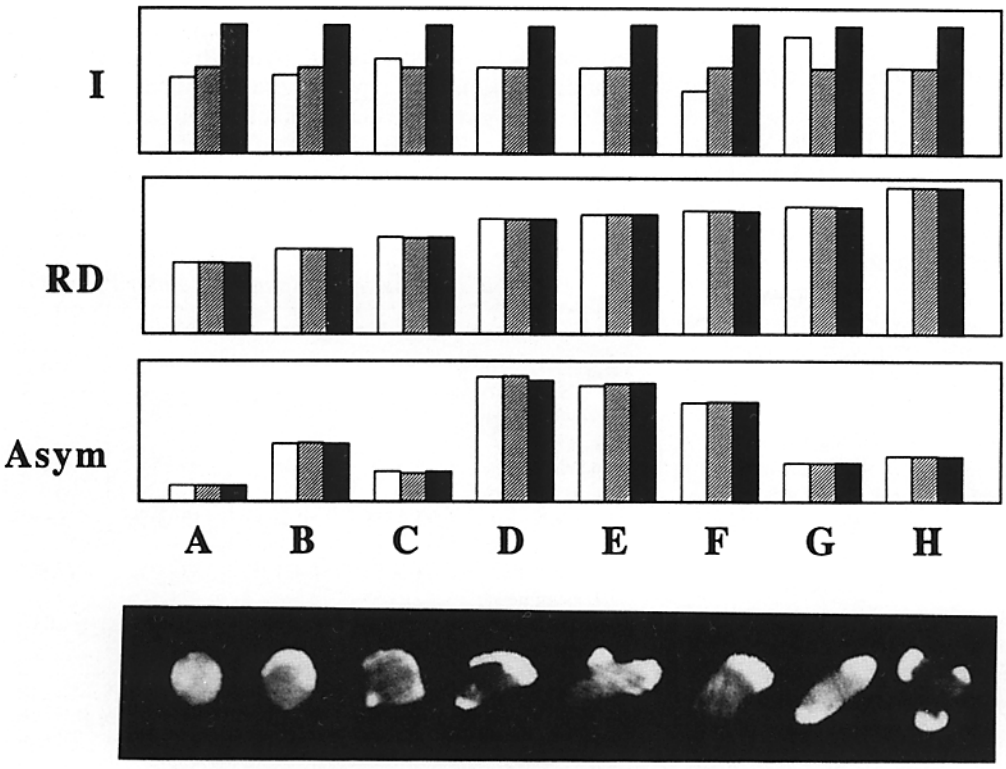

Figure 4. Relation of ASYM and RD to fluorescence distribution in selected PMN. The row of NBD-phal/TR ratio images (*A–H*) is a representative selection of the range of F-actin distributions observed in FMLP-activated PMN. The bar graphs show total fluorescence intensity (*I*), radial dispersion (*RD*), and asymmetry (*ASYM*) or cells A–H. The open bars are measurements made on the original set of images, shown at the bottom. The hatched bars represent measurements made on images normalized to the same total intensity and the solid bars are measurements on images adjusted to 1.5 × the normalized intensity. Only the original set of images is shown. The cells have been arranged in order of increasing RD.

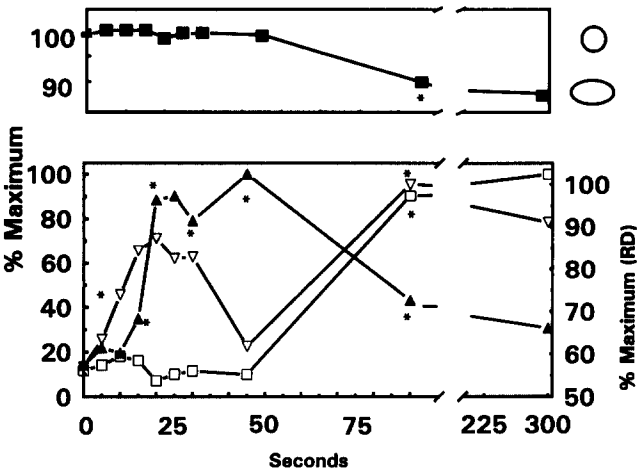

Figure 5. Changes in shape and F-actin distribution in PMN stimulated with 10^{-9} M FMLP. For comparison, the results of change in *ELIP* (■), total F-actin (▲), *RD* (▽), and *ASYM* (□) are expressed as percent of their maximum values. * indicates the point is significantly different from the previous point ($p < 0.01$).

cates that the parameters *ASYM* and *RD* are independent of total cellular fluorescence and are sensitive only to the distribution of fluorescence. These data show that the numerical parameters, calculated from fluorescence measurements of ratio images, appropriately describe fluorescence distribution. Therefore, total fluorescence intensity (*I*) is a measure of total F-actin, *RD* measures displacement of F-actin away from the cell center (whether symmetric or asymmetric), and *ASYM* measures only asymmetric distribution of F-actin, independent of the total F-actin content. These parameters qualitatively and quantitatively represent distribution of F-actin in PMN and are suitable for study of the kinetics of actin polymerization and the relation of F-actin distribution to shape change.

Kinetic Study of F-actin Redistribution and Shape Change after Stimulation

The NBD-phal/TR ratio images, obtained from PMN stimulated with 10^{-9} M FMLP at 25°C, were sampled and fixed at 5-s intervals, and were quantified on numerous cells ($n \cong$ 140 per time point) as described above. These conditions were chosen to allow maximum change in F-actin content, F-actin distribution, and shape (15). Since the distribution of the parameters is not Gaussian, median values of the changes in F-actin distribution at each time point were graphed. A representative of four data sets is shown in Fig. 5. In an initial phase of actin polymerization, total F-actin (*I*) rapidly increased, peaked at 25 s, and then decreased significantly by ~30 s. This transient decrease in F-actin was followed by a second polymerization phase which peaked at ~45 s. This biphasic pattern of total F-actin was prominent in all (n = 4) data sets analyzed by ratio imaging. *ELIP* was maximal during the first 45 s, indicating the cells remained round. During the first phase of polymerization, *RD* also increased while *ASYM* remained the same as control. This demonstrates that actin polymerization occurs preferentially at the edge of the round PMN and precedes development of asymmetric F-actin distribution. During the second phase of actin polymerization, *RD* decreased markedly at 45 s while F-actin approached its maximum. Since total F-actin was increasing, the concomitant decrease in *RD* can only be explained by a relative increase in F-actin near the center of the cell. This would be consistent with continued thickening of the peripheral mantle of F-actin. At times beyond 45 s, both *RD* and *ASYM* increased significantly, indicating that F-actin redistributes asymmetrically from the center of the PMN, as might be expected in a cell with a dominant pseudopod. As asymmetric distribution of F-actin developed between 45 and 90 s, F-actin depolymerization occurred and the PMN changed shape from round to polar, as implied by a decrease in *ELIP*. At 300 s, while *ASYM* was maximum, total F-actin decreased. These data show that appearance of an asymmetric F-actin distribution coincides with and may precede shape change.

NBD-phal/TR Ratio Images

Since it is not possible to follow change in F-actin distribution sequentially in a statistically significant number of individual neutrophils, it is difficult to directly determine if temporal development of asymmetric F-actin distribution precedes or perfectly coincides with appearance of polar shape. However, if asymmetric F-actin distribution precedes transition to polar shape, then two conditions should be satisfied as polar shape appears: (1) there must be round PMN with asymmetric F-actin distribution, and (2) all polar cells must have asymmetric F-actin distribution. To determine whether these conditions are met in PMN, we used extremely restrictive, statistically derived definitions of shape and asymmetric F-actin distribution which were based upon measurements of PMN at time 0. Defining these parameters on time 0 cells assures the most restrictive definition of round cells and of asymmetric F-actin distribution and the least restrictive definition of a polar cell. For this analysis, a round cell was defined as a cell with *ELIP* ≥ upper 25th percentile and a polar cell as one with *ELIP* ≤ lower 25th percentile of time 0 PMN. The upper 95th percentile value of ASYM was used as the cutoff between asymmetric and symmetric actin distribution. We applied these definitions to look for asymmetric F-actin distribution in round cells and polar cells at times ≥45 s (Table I). At 45 s, 100% of round cells and 95% of polar cells have symmetric F-actin distribution. At all time ≥90 s, the F-actin distribution is asymmetric in

Table I. F-actin Distribution in Round and Polar PMN

Shape and distribution*	Time after stimulation			
	0 s	45 s	90 s	300 s
Round PMN that are symmetric	96.67%	100%	6.25%	0%
Round PMN that are asymmetric	3.33%	0%	93.75%	100%
Polar PMN that are symmetric	95.65%	95%	13.00%	2.08%
Polar PMN that are asymmetric	4.35%	4.17%	87.00%	97.92%
Total PMN per time point	98	189	146	203

* Defined for all time points based upon PMN at 0 s after stimulation. "Round" and "polar" are defined as ellipticity ≥ the 75th percentile or ≤ 25th percentile, respectively. "Symmetric" and "asymmetric" are defined as ASYM < 95th percentile or ≥ 95th percentile, respectively.

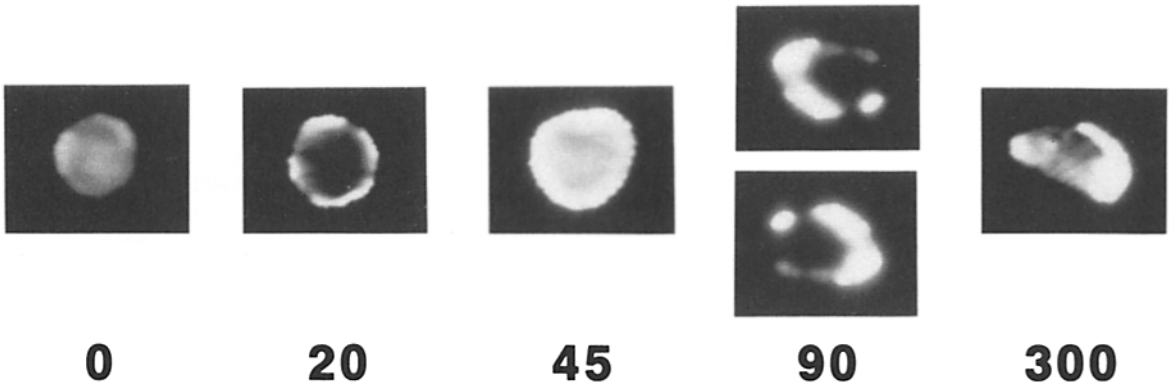

Figure 6. Ratio images of PMN at critical time points after stimulation. Images were selected based upon statistical criteria as described in the text. The orientation of the 90-s images could not be determined based upon ASYM alone.

≥94% of round cells and ultimately in all (98%) of polar PMNs. These results show that as polar shape appears, all polar cells and the roundest of round cells exhibit asymmetric F-actin distribution. This result strongly suggests that asymmetric distribution of F-actin occurs before development of polar shape.

Relationship of F-actin Content, F-actin Distribution, and Cell Shape to Pseudopod Development

To picture the sequence of events occurring as F-actin distribution changes and shape change occurs, we obtained representative images at each time point from the kinetic experiments. The most common value (mode) of each of the distribution parameters was calculated for each time point (~100–200 cells per time point per experiment) and representative PMN with values of *I*, *RD*, *ASYM*, and *ELIP* at their respective modes were displayed. Thus, only cells with the most common total F-actin, F-actin distribution, and cell shape at each time point were selected for viewing and are presented in Fig. 6, as a visual representation of the numerical parameters shown in Fig. 5. Up to 45 s, the most representative cells remain round while F-actin is polymerized circumferentially. Beyond 45 s, the distribution of F-actin becomes asymmetric, polarization occurs, and an actin-rich pseudopod appears (Fig. 6). The fact that *ASYM* increased at 90 s showed that F-actin was localized to one end of the cell. One might assume the F-actin is asymmetrically distributed into the pseudopod. However, the value of *ASYM* only shows that the F-actin is asymmetrically distributed and does not determine the position of F-actin asymmetry in relation to the pseudopod. Because of this uncertainty, the orientation of the fluorescence is pictured both toward the front and toward the back of the cell at 90 s in Fig. 6. Further analysis was required to determine which orientation comes first.

We assumed the pseudopod was the thinnest part of the cell and determined the relationship between F-actin location, measured by NBD-phal distribution, and the thickness of the cell, measured by TR distribution. To confirm this assumption for nascent pseudopods as well as fully developed pseudopods, two experiments were performed. First, 90-s time point TR images were manually selected such that early pseudopod formation was present. Fluorescence intensity over the early pseudopod was 70 ± 14% of the cell body (n = 54), indicating the early pseudopod is thinner. Second, live PMN were loaded with FURA-2 (24) and recorded on optical disk during spontaneous pseudopod extension. This was done by video image analysis on a fluorescence microscope equipped with temperature controlled stage (37°C). Fluorescence was excited at the calcium-insensitive wavelength of FURA-2 (355 nm) so that fluorescence intensity would approximate cell thickness. The fluorescence intensity over the nascent pseudopods, which could be clearly identified by running the recording in reverse and watching the fully developed pseudopod retract, was lower than that of the cell body. In measurements of equal-sized regions of cell body and nascent pseudopod from 25 PMN, the intensity over the pseudopod was 4,337 ± 690 and 6,177 ± 488 over the cell body. This is in good agreement with the TR data above. These experiments corroborate other observations of PMN pseudopod extension from the literature (20, 25, 35) and show that the developing pseudopod is indeed thinner than the cell body. To demonstrate the relation between developing pseudopod and F-actin location, we defined a vector, $\bar{I}$, which originates at the geometric center of the cell and points toward the brightest region of the image. When determined from the NBD-phal/TR ratio image, $\bar{I}$ points to the end of the cell with the most F-actin per unit volume ($\bar{I}_{ratio}$). When applied to the TR image only, the vector ($\bar{I}_{TR}$) points to the thickest part of the cell, i.e., the end opposite the pseudopod. The vector dot product of the $\bar{I}_{TR}$ and the $\bar{I}_{ratio}$ vectors can be calculated (see Materials and Methods). A dot product greater than zero results when the vectors point in the same direction, indicating that the F-actin is in the thick end of the cell. Conversely, a value less than zero results if the two vectors point in the opposite direction, suggesting that the F-actin concentration is greatest in the pseudopod. These calculations were applied to polar cells at two critical time points. At 90 s, 66% of the polarized cells had a positive dot product. By 300 s, the dot product was positive in 29% of the cells (Fig. 7). Therefore, the F-actin concentration at 90 s was lowest at the site of the developing pseudopod while, by 300 s, the F-actin concentrated in the thinner end of cell, i.e., in the end of the fully developed pseudopod. This analysis suggests that orientation of F-actin distribution at 90 s is most accurately depicted by the upper picture in Fig. 6.

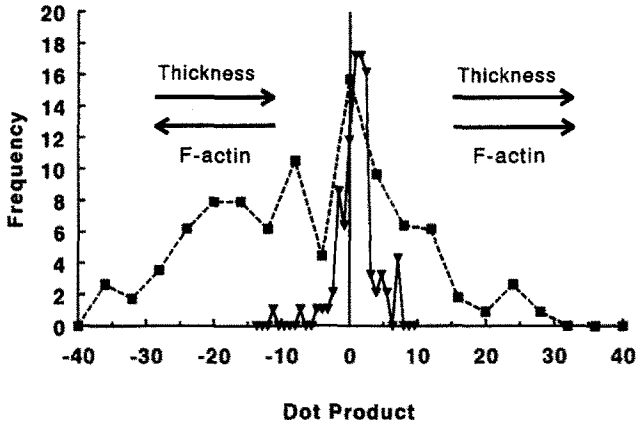

Figure 7. Frequency histogram of the dot product between $\bar{I}_{ratio}$ and $\bar{I}_{TR}$ in polar PMN. Approximately 66% of the cells at 90 s (▼) have a positive dot product while only 29% of the cells at 300 s (■) have a positive dot product. The larger range of values of the dot product at 300 s primarily reflects the greater magnitude of $\bar{I}_{ratio}$ (*ASYM*) at that time. The positive dot product indicates cells with F-actin concentrated in the thick part of the cell. A negative dot product indicates F-actin is concentrated in the thinner part of the cell.

Discussion

This paper describes direct measurements of shape and fluorescence which permit a quantitative kinetic study of the temporal relationship between changes in F-actin content, F-actin distribution, and acquisition of polar shape in chemotactic peptide-activated PMN in suspension. There are four distinct experimental and methodological advantages of this study over previous studies of the role of the microfilamentous cytoskeleton in determining nonmuscle cell shape. First, the PMN shape changes are studied in suspension and therefore reflect only the effect of intrinsic cytoskeletal rearrangements on shape. Second, the PMN studied are endotoxin free and therefore are initially smooth-surfaced, spherical cells which can subsequently assume any shape after chemotactic factor activation (35). Third, the video imaging techniques used to measure F-actin content and distribution from ratio images of PMN permit estimation of F-actin content per unit volume, thus compensating for variation of cell thickness in determination of F-actin distribution. Use of ratio imaging permits observation of asymmetric distribution of F-actin in round cells. Finally, unlike many morphologic studies which rely on examination of "representative" cells to determine shape and F-actin parameters, the computerized video image analysis applied here allows objective direct measurement of shape and distribution on samples of cells which are large enough for statistical analysis. The technology therefore permits conclusions based on average or median behaviors as well as study of heterogeneity of polarization, and F-actin distribution.

The ideal way to determine the relation of F-actin localization to shape change and pseudopod development would be to study F-actin distribution sequentially in a single neutrophil as the pseudopod extends. Unfortunately, this is not possible in PMN with current methods of detecting F-actin. We approached the problem by studying PMN at fixed time points after stimulation using mathematical parameters which we developed to quantitatively describe the F-actin distribution in individual PMN. The goal was to develop useful numbers that permit definition of shape and F-actin distribution in a statistical sense rather than to develop parameters that are sensitive to the fine details of F-actin distribution and cell shape. *ASYM*, *RD*, and the intensity vector, $\bar{I}$, are measures of F-actin distribution which describe the average characteristics of the F-actin distribution throughout the cell and ignore contributions of F-actin in small blebs and protrusions except as they contribute to the average. Similarly, *ELIP*, as a measure of shape, is sensitive only to global deviation from a round shape but has been useful in recognition of polarized PMN with a dominant pseudopod (15). Shape descriptors exist (7) which permit quantification of finer details of early pseudopod formation, such as bleb formation (35); however, ways to adapt these measures to kinetic analysis have not been developed. Nonetheless, as we have shown, the parameters developed here are able to detect changes in stimulated PMN which relate distribution of F-actin to change in shape. This ability is due, in part, to the fact that relatively large numbers of PMN were studied in an unbiased manner.

The sequence of events determined derived from the kinetic study of *RD*, *ASYM*, and *ELIP* is consistent with the previously suggested role for F-actin polymerization in causing the polar shape (22, 31, 35). Our studies show that radial distribution of F-actin in a nonpolarized cell precedes, and development of an asymmetric F-actin distribution occurs coincident with, development of polar shape. While this sequence is consistent with a role for F-actin in the development of polar shape, it does not prove that change in distribution of F-actin is necessary for change in shape. However, our data showing asymmetric F-actin distribution in round cells 90 s after FMLP activation demonstrates that asymmetric distribution of F-actin can precede appearance of polar shape. This observation paired with the fact that virtually 100% of polar cells at 90 and 300 s exhibit asymmetric F-actin distribution make it unlikely that polar shape can occur without asymmetric distribution of F-actin. The results strongly suggest that development of asymmetric F-actin distribution precedes and is causally related to development of polar shape in PMN.

The kinetics shown in Fig. 5 suggest there are two phases of actin polymerization which accompany changes in F-actin distribution. The first phase of actin polymerization lasts 25 s, occurs circumferentially around the cell center as evidenced by the increase in *RD*, and is likely localized to the subcortical region of the cell as shown by representative photographs in Fig. 5. The increase in *RD* is consistent with polymerization starting in the submembranous region of the cell as has recently been shown in fibroblast lamellipodia (30). The second phase of actin polymerization begins after 30 s and reaches a maximum at 45 s. FACS analysis concurrent with these studies (not shown) corroborates the observed two rates of actin polymerization. Interestingly, examination of published F-actin data by flow cytometry also demonstrates two phases of polymerization in PMN (12, 26) and macrophages (9) though the observation is not discussed at length. This second phase of actin polymerization occurs nearer the cell center as evidenced by a decrease in *RD* and a uniform increase in F-actin throughout the cell as seen in the representative photograph of a PMN at 45 s after stimulation (Fig. 6). Biphasic polymerization kinetics have also

been seen in *Dictyostelium discoideum* amebocytes, in suspension, and on surfaces. In these cells, the later phase of polymerization was associated with appearance of F-actin in the pseudopod and development of polar shape (6, 11). Whether these two phases in PMN simply represent oscillations in actin polymerization (21, 36) or could be related to two pools of actin with differing kinetics of polymerization (3, 5, 34) remains to be determined.

Several models have been proposed to explain how the force is developed to cause protrusion of a pseudopod. These models involve force produced by polymerization of the actin itself, filament sliding due to interaction with myosin, and gel swelling due to the formation and dissolution of a hydrated actin gel (6, 23, 29). The sequence of events determined here by ratio imaging (Fig. 6) is consistent with a model of pseudopod extension based upon osmotic forces. In this model, force is generated as actin is severed leading to increased osmotic pressure and focal swelling (23). Our data show that actin polymerizes symmetrically and rapidly concentrates in a rim at the cortex. The decrease in F-actin at 30 s could contribute to osmotically induced water influx though sodium influx occurs at this time as well and accounts for about two thirds of the measured volume change in PMN after stimulation with FMLP (10). The increase in *ASYM* as F-actin decreases at 90 s suggests that asymmetry develops because of net loss in F-actin. The fact that the dot product (Fig. 7) is mainly positive implies that this loss is in the region of the developing pseudopod. The change in sign of the dot product by 300 s (Fig. 7) represents polymerization in the end of the developing pseudopod. Since total F-actin stays the same, there must be loss of F-actin from other regions of the cell as well. We chose the "protein space" indicated by TR as the denominator for representation of the distribution of F-actin used to determine these relations. In fact, the cortex thickness exclusive of organelles may be a better distribution space as organelles move into the developing pseudopod. The TR protein space we used would underestimate F-actin concentration in organelle-rich regions. While this may alter the magnitude of certain distribution measures, F-actin would still have to decrease at the point of pseudopod extrusion to obtain the vector relations in Fig. 7. Organelles may move into the region of the nascent pseudopod because of focal F-actin loss. This model does not require a gradient but does assume that some asymmetry in thickness of the F-actin rim initiates development of the dominant pseudopod. The cause of the initial asymmetry remains undetermined. A gradient of attractant or the presence of surface contact would impose asymmetry on activated PMN and direct the extension of the pseudopod.

This data does not prove that osmotic forces alone cause pseudopod protrusion and does not preclude contributions from contractile elements such as myosin. While myosin is not abundant in PMN, myosin light chain kinase is phosphorylated after stimulation of PMN by FMLP (2). If focal depolymerization of the cortical actin rim precedes pseudopod protrusion, then contraction would increase the core pressure and enhance the actomyosin-dependent flow of cytoplasm toward the weakened area of the cortex.

The studies presented here demonstrate quantitatively that development of asymmetry of F-actin distribution is closely related to and probably precedes development of polar shape in human PMN stimulated in suspension with 10^{-9} M FMLP. Furthermore, after net F-actin has increased symmetrically at the PMN edge, the dominant pseudopod develops in the region of lowest F-actin content. This is followed by polymerization of actin in the end of the developed pseudopod as has been suggested (29). The sequence of events presented here leaves many questions unanswered, particularly regarding the mechanism of the changes seen. The kinetics and distribution of gelsolin and other actin regulatory proteins, for example, undoubtedly play a role (17) in determining F-actin distribution. The mathematical tools developed here for F-actin provide a method for kinetic study of the spatial relation between critical morphologic features of the cell and can be used to address some of these remaining questions.

The authors wish to thank Dr. Martine Torres for her input and critical review of the manuscript.

This work was supported by National Institutes of Health grants AI23547 (T. D. Coates), AI25214 (T. H. Howard), and K11-HL02601 (R. G. Watts) and American Cancer Society grant IRG 66-31. Dr. Watts is a Fellow of the Dixon Foundation, Birmingham, AL. Dr. Howard is an Established Investigator of the American Heart Association.

Received for publication 10 October 1991 and in revised form 13 February 1992.

References

1. Ayres, F., Jr. 1969. Schaum's Outline Series: Theory and Problems of Matrices. McGraw-Hill Inc., New York. 100 pp.
2. Blikstad, I., and L. Carlsson. 1982. On the dynamics of the microfilament system in HeLa cells. *J. Cell Biol.* 93:122–128.
3. Brennan, P. J., S. H. Zigmond, A. D. Schreiber, E. R. Smith, and F. S. Southwick. 1991. Binding of IgG containing immune complexes to human neutrophil FcgammaRII and FCgammaRIII induces actin polymerization by a pertussis toxin-insensitive transduction pathway. *J. Immunol.* 146:4282–4288.
4. Bright, G. R., G. W. Fisher, J. Rogowska, and D. L. Taylor. 1989. Fluorescence ratio imaging microscopy. *In* Methods in Cell Biology: Fluorescence Microscopy of Living Cells in Culture, Part B. Academic Press Inc., San Diego, CA. 157–190.
5. Cassimeris, L., H. McNeill, and S. H. Zigmond. 1990. Chemoattractant-stimulated polymorphonuclear leukocytes contain two populations of actin filaments that differ in their spatial distributions and relative stabilities. *J. Cell Biol.* 110:1067–1075.
6. Condeelis, J., A. Bresnick, M. Demma, S. Dharmawardhane, R. Eddy, A. L. Hall, R. Sauterer, and V. Warren. 1990. Mechanisms of ameboid chemotaxis: an evaluation of the cortical expansion model. *Dev. Genet.* 11:333–340.
7. Diaz, G., D. Quacci, and C. Dell'Orbo. 1990. Recognition of cell surface modulation by elliptic Fourier analysis. *Comput. Methods Program. Biomed.* 31:57–62.
8. Fechheimer, M., and S. H. Zigmond. 1982. Changes in cytoskeletal proteins of polymorphonuclear leukocytes induced by chemotactic peptides. *Cell Motil.* 3:349–361.
9. Greenberg, S., J. El Khoury, F. Di Virgilio, E. M. Kaplan, and S. C. Silverstein. 1991. Ca^{2+}-independent F-actin assembly and disassembly during Fc receptor-mediated phagocytosis in mouse macrophages. *J. Cell Biol.* 113:757–767.
10. Grinstein, S., W. Furuya, and E. J. Cragoe. 1986. Volume changes in activated human neutrophils: the role of Na+/H+ exchange. *J. Cell. Physiol.* 128:33–40.
11. Hall, A. L., A. Schlein, and J. Condeelis. 1988. Relationship of pseudopod extension to chemotactic hormone-induced actin polymerization in amoeboid cells. *J. Cell Biochem.* 37:285–299.
12. Harvath, L. 1990. Regulation of neutrophil chemotaxis: correlations with actin polymerization. *Cancer Invest.* 8:651–654.
13. Haughland, R. P. 1990. Fluorescein substitutes for microscopy and imaging. *In* Optical Microscopy for Biology. B. Herman and K. Jacobson, editors. Wiley-Liss, Inc., New York. 143–157.
14. Hiraoka, Y., J. W. Sedat, and D. A. Agard. 1990. Determination of three-dimensional imaging properties of a light microscope system. Partial confocal behavior in epifluorescence microscopy. *Biophys. J.* 57:325–333.
15. Howard, T. H., and C. O. Oresajo. 1985. The kinetics of chemotactic peptide-induced change in F-actin content, F-actin distribution, and the shape of neutrophils. *J. Cell Biol.* 101:1078–1085.
16. Howard, T. H., and C. O. Oresajo. 1985. A method for quantifying F-actin

in chemotactic peptide activated neutrophils: study of the effect of tBOC peptide. *Cell Motil.* 5:545–557.
17. Howard, T., C. Chaponnier, H. Yin, and T. Stossel. 1990. Gelsolin-actin interaction and actin polymerization in human neutrophils. *J. Cell Biol.* 110:1983–1991.
18. Howard, T. H., D. Wang, and R. L. Berkow. 1990. Lipopolysaccharide modulates chemotactic peptide induced actin polymerization in neutrophils. *J. Leukocyte Biol.* 47:13–24.
19. MacFarlane, G. D., M. C. Herzberg, and R. D. Nelson. 1987. Analysis of polarization and orientation of human polymorphonuclear leukocytes by computer-interfaced video microscopy. *J. Leukocyte Biol.* 41: 307–317.
20. Murray, J., H. Vawter-Hugart, E. Voss, and D. R. Soll. 1992. A three dimensional motility cycle in leukocytes. *Cell Motil. Cytoskeleton.* In press.
21. Nathan, C., and E. Sanchez. 1990. Tumor necrosis factor and CD11/CD18 (β2) integrins act synergistically to lower cAMP in human neutrophils. *J. Cell Biol.* 111:2171–2181.
22. Oliver, J. M., J. A. Krawiec, and E. L. Becker. 1978. The distribution of actin during chemotaxis in rabbit neutrophils. *J. Reticuloendothel. Soc.* 24:697–704.
23. Oster, G. F., and A. S. Perelson. 1987. The physics of cell motility. *J. Cell Sci.* 8(Suppl.):35–54.
24. Scanlon, M., D. A. Williams, and F. S. Fay. 1987. A Ca+2-insensitive form of Fura-2 associated with polymorphonuclear leukocytes. *J. Biol. Chem.* 262:6308–6312.
25. Senda, N., H. Tamura, N. Shibata, J. Yoshitake, K. Kondo, and K. Tanaka. 1975. The mechanism of leukocyte of the movement of leukocytes. *Exp. Cell Res.* 91:393–407.
26. Sklar, L. A., G. M. Omann, and R. G. Painter. 1985. Relationship of actin polymerization and depolymerization to light scattering in human neutrophils: dependence on receptor occupancy and intracellular Ca++. *J. Cell Biol.* 101:1161–1166.
27. Southick, F. S., G. A. Dabiri, M. Paschetto, and S. H. Zigmond. 1989. Polymorphonuclear leukocyte adherence induces actin polymerization by a transduction pathway which differs from that used by chemoattractants. *J. Cell Biol.* 109:1561–1569.
28. Stossel, T. P. 1989. From signal to pseudopod. How cells control cytoplasmic actin assembly. *J. Biol. Chem.* 264:18261–18264.
29. Stossel, T. P. 1990. How cells crawl. *Am. Sci.* 78:408–423.
30. Symons, M. H., and T. J. Mitchison. 1991. Control of actin polymerization in live and permeabilized fibroblasts. *J. Cell Biol.* 114:503–513.
31. Wallace, P. J., R. P. Wersto, C. H. Packman, and M. A. Lichtman. 1984. Chemotactic peptide-induced changes in neutrophil actin conformation. *J. Cell Biol.* 99:1060–1065.
32. Wang, Y. L. 1987. Mobility of filamentous actin in living cytoplasm. *J. Cell Biol.* 105:2811–2816.
33. Watson, P. A. 1991. Function follows form: generation of intracellular signals by cell deformation. *FASEB (Fed. Am. Soc. Exp. Biol.) J.* 5:2013–2019.
34. Watts, R. G., and T. H. Howard. 1992. Evidence for a gelsolin-rich, labile F-actin pool in human polymorphonuclear leukocytes. *Cell Motil. Cytoskeleton.* 21:25–37.
35. Watts, R. G., M. A. Crispens, and T. H. Howard. 1991. A quantitative study of the role of F-actin in producing neutrophil shape. *Cell Motil. Cytoskeleton.* 19:159–168.
36. Wymann, M. P., P. Kernen, T. Bengtsson, T. Andersson, M. Baggiolini, and D. A. Deranleau. 1990. Corresponding oscillations in neutrophil shape and filamentous actin content. *J. Biol. Chem.* 265:619–622.
37. Zigmond, S. H., H. I. Levitsky, and B. J. Kreel. 1981. Cell polarity: an examination of its behavioral expression and its consequences for polymorphonuclear leukocyte chemotaxis. *J. Cell Biol.* 89:585–592.